Understanding the mechanism of cargo recognition by the Ssh4-Rsp5 ubiquitin ligase complex at the yeast vacuole membrane

Honors Thesis
Presented to the College of Arts and Sciences,
Cornell University
in Partial Fulfillment of the Requirements for the
Biological Sciences Honors Program

by
Jonathan Weng
May 2019

Supervisor: Scott Emr

Abstract

The preservation of a healthy proteome is important for all cellular function. Sequential protein quality control (QC) mechanisms along the endocytic pathway safeguard the identity of different organelles by eliminating damaged or mislocalized proteins. In *Saccharomyces cerevisiae*, the Rsp5 ubiquitin ligase is required for cargo ubiquitination at all steps of endocytic QC, and its activity is mediated by its recruitment to organelle membranes by specific adaptors. The ART adaptor network directs Rsp5 to the plasma membrane (PM), while the intracellular adaptor Ssh4 recruits it to the vacuole membrane (VM). This study shows that PM proteins mistargeted to the VM are recognized and sorted by the Ssh4-Rsp5 complex and that Ssh4 contains important features that facilitate its cargo sorting. Furthermore, Ssh4-Rsp5-mediated QC employs a seemingly promiscuous mechanism of cargo recognition at the VM. Finally, targeting Ssh4 to the PM induces some non-specific degradation of PM proteins that are accessible to Ssh4-Rsp5.

Introduction

Cellular life heavily relies on the maintenance of a healthy proteome, and central to this homeostatic regulation are protein quality control (QC) pathways. The cell must be able to differentiate between native and aberrant proteins, since the aggregation of damaged or mislocalized membrane proteins can interfere with normal cellular function by disrupting essential membrane processes or membrane permeability. A complex series of organelle-specific QC mechanisms therefore exists to monitor the quality, quantity, and localization of proteins (MacGurn et al., 2012). These sequential QC systems oversee the movement of membrane proteins as they traffic through multiple compartments in their lifetime. One well-studied QC step is endoplasmic reticulum (ER)-associated degradation (ERAD), during which permanently misfolded membrane and secretory proteins in the ER are recognized and targeted for proteasomal elimination in the cytoplasm (Berner et al., 2018). In contrast, most post-ER QC processes target aberrant proteins for degradation to the lysosome (MacGurn et al., 2012).

Rsp5, the lone member of the human Nedd4 E3 ubiquitin ligase family in *Saccharomyces cerevisiae*, performs a crucial role in ubiquitin-mediated membrane protein trafficking. Ubiquitin is a 76-amino acid (aa) peptide that can be conjugated to the lysine residue of a recipient protein and acts as a signal for endocytosis and sorting, among other functions. Rsp5 is recruited to different organelles by specialized adaptor proteins, enabling Rsp5 to access and ubiquitinate the cytosolic domains of a broad range of membrane proteins at multiple cellular locations. At the same time, the dependence of Rsp5 on adaptors for substrate accessibility also serves to regulate Rsp5 activity (Léon and Haguenauer-Tsapis, 2009). At the PM, a network of arrestin-related trafficking adaptors (ARTs) regulates Rsp5-mediated clearance of damaged or misfolded proteins that accumulate upon environmental stress (Lin et al., 2008; Zhao et al., 2013). Rsp5-

mediated sorting of intracellular cargos is facilitated by adaptors such as Ssh4 at the vacuole membrane (VM) and Ear1 at the endosomal membrane (Belgareh-Touzé et al., 2008). Ubiquitinated cargos are ultimately packaged by endosomal sorting complexes required for transport (ESCRTs) into vesicles that bud into the lumen of endosomes or vacuoles (Henne et al., 2013; Piper et al., 2014).

While considerable research has been conducted into the downstream mechanisms of cargo sorting for degradation, we still lack insight into the process of cargo recognition by Rsp5 adaptors. The Emr Lab has previously shown that endocytosed PM cargos that escape multivesicular body (MVB) sorting can be recognized by Ssh4-Rsp5 E3 ubiquitin ligase at the VM (Sardana et al., 2018). In this work, I was interested in probing the features of Ssh4 that provide the specificity for recognition of diverse PM proteins on the VM. I demonstrate that the PY motifs and splA/ryanodine receptor (SPRY) domain of Ssh4 are important for its function in cargo sorting. Additionally, when selecting the lysine residue on the cargo to be ubiquitinated, the Ssh4-Rsp5 complex at the VM shows promiscuity in its selection. Finally, I wanted to examine whether targeting Ssh4 to other organelles would result in non-specific degradation of resident membrane proteins. I show that targeting Ssh4 to the PM engenders some non-specific degradation of PM proteins in close proximity to Ssh4, although the exact qualifications for this degradation are not fully understood.

Results

Tagging PM proteins with an acidic dileucine motif mistargets them to the vacuole

Work from the Emr Lab has demonstrated that the Ssh4-Rsp5 adaptor-E3 ubiquitin ligase complex can recognize and ubiquitinate PM proteins that escape MVB sorting and aberrantly

reach the VM (Sardana et al., 2018). These ubiquitinated proteins are then sorted for degradation by proteases into the vacuole lumen. To understand the features of Ssh4 that are important for cargo recognition, I devised a strategy to biosynthetically redirect PM-bound proteins to the VM by fusing PM cargos with an acidic dileucine (acLL) motif (NEQSPLL; Darsow et al., 1998), which is recognized by the AP-3 adaptor complex at the Golgi apparatus and directed to the vacuole (Figure 1A; Cowles et al., 1997; Vowels and Payne, 1998). I shortlisted multiple PM proteins with varied topologies and transmembrane domains (TMDs) and tagged them with the acLL motif as well as GFP for visualization by fluorescence microscopy. Although addition of the acLL motif did not affect the localization of many of the tested proteins, I found that Mup1-acLL-GFP and Wsc1-acLL-GFP were successfully rerouted to the vacuole, accumulating in the vacuole lumen at steady state (Figures 1B and S1). Mup1 is a high affinity methionine permease with 12 TMDs (Isnard et al., 1996; Guiney et al., 2016), while Wsc1 is a cell surface integrity sensor with a single TMD (Philip and Levin, 2001). Endocytosed Mup1 and Wsc1 have been recently shown by our lab to be recognized by Ssh4-Rsp5 at the VM (Sardana et al., 2018). I therefore employed acLL-tagged Mup1 and Wsc1 as reporters to understand protein degradation at the VM.

PY motifs and SPRY domain of Ssh4 are important for its function in cargo sorting

The steady-state localization of the acLL-tagged reporters in the vacuole lumen suggested that the rerouted cargos were being recognized as aberrant proteins at the VM and sorted for degradation in the lumen. I hypothesized that the misdirected proteins were recognized by Ssh4-Rsp5 at the VM. Indeed, when expressed in an *ssh4*Δ mutant strain, the Wsc1-acLL-GFP reporter was blocked on the VM as visualized by fluorescence microscopy (Figure 2A).

Additionally, since GFP is resistant to vacuolar hydrolases, vacuolar degradation of the reporter could also be assayed via western blotting by observing the accumulation of free GFP. While I observed accumulation of free GFP in wild-type (WT) cells, degradation was strongly blocked in the *ssh4*Δ mutant (Figure 2B). Without Ssh4, Rsp5 is likely unable to recognize and target the aberrant protein reporter for degradation.

Rsp5 E3 ubiquitin ligase is a cytosolic protein that is recruited to its target substrates on organelle membranes by an interaction between the WW domains of Rsp5 and PY motifs (PPxY, where x is any aa). However, most targets of Rsp5 do not themselves contain the PY motif; instead, their interaction with Rsp5 is mediated by an adaptor protein that possesses PY motifs. Adaptor proteins, including Ssh4, interact with the WW domains of Rsp5 through their PY motifs and thereby recruit Rsp5 to the target organelle (MacGurn et al., 2012; Léon et al., 2008). Ssh4 has a single TMD and localizes to the VM. In addition to a SPRY domain, it contains two PY motifs in its cytosolic region (Figure 3A). I assessed the different regions of Ssh4 required for cargo degradation at the VM.

To confirm that the PY motifs of Ssh4 are necessary for proper cargo sorting at the VM, I constructed an $Ssh4^{PY}$ mutant by mutating both PPxY motifs to PAxA. *ssh4*Δ cells expressing Wsc1-acLL-GFP and the $Ssh4^{PY}$ mutant construct exhibited a block of the reporter on the VM (Figure 3B and C), indicating that cargo sorting to the vacuole lumen requires functional PY motifs of Ssh4.

Next, I studied the requirement of the SPRY domain in the cytosolic region of Ssh4 for cargo sorting. The SPRY domain is a conserved immunoglobulin-like fold often involved in protein-protein interactions (D'Cruz et al., 2013; Woo et al., 2006). The endosomal adaptor of Rsp5, Ear1, shares a similar architecture and 43% sequence similarity (25% identity) with Ssh4

(Léon et al., 2008). Ssh4 and Ear1 each contain a SPRY domain (Figure S2A), and the sequences of the two domains share 38% identity (Figure S2B). While Ssh4 localizes and recruits Rsp5 to the VM, Ear1 is an endosomal membrane adaptor of Rsp5. Endocytosed PM proteins that escape MVB sorting are sequentially monitored and recognized by Ear1-Rsp5 at the endosome and Ssh4-Rsp5 at the vacuole (Sardana et al., 2018). This tiered system suggests that the mechanisms of cargo recognition by the two adaptors may be similar. The high conservation between the two adaptors led me to hypothesize that proper adaptor function may still be maintained after swapping their SPRY domains. The SPRY domain of WT Ssh4 was thus swapped with the SPRY domain of Ear1 to generate an Ssh4-Ear1^{SPRY} construct (Figure 4A) that was then expressed in *ssh4*Δ cells also expressing Wsc1-acLL-GFP. Although the localization and stability of Ssh4-Ear1^{SPRY} were similar to those of WT Ssh4, Ssh4-Ear1^{SPRY} was completely non-functional for cargo sorting (Figure 4B-D). Taken together, the SPRY domain and PY motifs of Ssh4 play important roles in the recognition of protein cargos and recruitment of Rsp5 to the VM, respectively, for efficient cargo degradation at the VM.

Ssh4-Rsp5 shows promiscuity in selecting accessible lysine residues on the cargo for ubiquitination

Both Mup1 and Wsc1 contain multiple lysine residues in their cytosolic regions that could presumably be ubiquitinated by the Ssh4-Rsp5 complex. I wanted to understand which residues act as key substrates for Ssh4-Rsp5-mediated ubiquitination at the VM. The cytosolic N-terminal tail of Mup1-acLL-GFP has four lysine residues at aa positions 16, 27, 28, and 59 (Figure S3). Considering the lysine at position 59 is only one residue away from the membrane, making it an unlikely ubiquitination target, I focused my attention on K16, K27, and K28. K27

and K28 have been previously shown to be required for Mup1 ubiquitination at the PM for endocytosis (Guiney et al., 2016). While individual mutation of K16, K27, or K28 to arginine did not block cargo degradation, mutating all three together blocked Mup1-acLL-GFP on the VM (Figure 5). These data, along with the recognition of lysine residues in Wsc1-acLL-GFP by the Ssh4-Rsp5 complex (Sardana et al., 2018), suggest that Ssh4-Rsp5 is promiscuous in lysine selection, so a single preferred residue likely does not exist as long as multiple accessible residues are available in a spatially restricted region.

Targeting Ssh4 to the PM induces non-specific degradation

This study has shown that the Ssh4-Rsp5 ubiquitin ligase complex is capable of clearing aberrant membrane proteins at the VM by employing a rather promiscuous target recognition mechanism. Since the vacuole is the terminal destination of the endocytic pathway, this fail-safe mechanism permits the recognition of diverse cargos and prevents aberrant build-up on the VM. I therefore wondered how targeting Ssh4 to other organelles would affect protein degradation and cellular fitness. I employed a few different approaches in attempting to mistarget Ssh4 to non-vacuolar locations in the cell. First, past studies have shown that a cytoplasmic dilysine (KKxx) motif directs Golgi-to-ER retrieval of type I membrane proteins (Gaynor et al., 1994; Benghezal et al., 2000). In seeking to mistarget Ssh4 to the ER, I affixed a KKTN motif to the C-terminal end of the adaptor (Figure 6A); however, the fusion construct failed to localize to the ER (Figure 6B). Next, previous work in the Emr Lab suggests that the C-terminal tail of Rcr1 contains a PM localization signal. I fused this tail sequence to Ssh4 (Figure 7A), but the fusion construct was not mistargeted to the PM as intended (Figure 7B). Furthermore, the vacuolar localization of the fusion construct even in an endocytosis-defective *end3*Δ mutant ruled out the

possibility that it was directed to the PM but constitutively endocytosed (Figure 7B). Finally, the FRB-FKBP system is a heterodimer formation system in which the association of FK506 binding protein (FKBP) and the FKBP-rapamycin binding (FRB) domain of the mammalian target of rapamycin (mTOR) kinase is inducible by rapamycin, an immunosuppressive drug that binds simultaneously to FKBP and FRB (Putyrski and Schultz, 2012; Inobe and Nukina, 2016). An earlier study from our lab developed the rapamycin-induced degradation (RapiDeg) system, by which a VM protein fused with FKBP was degraded upon addition of rapamycin and a chain of three ubiquitin molecules fused to FRB (Zhu et al., 2017). The strain lacked Fpr1 and contained the mutant *tor1-1*, allowing it to grow in the presence of rapamycin. I designed an analogous system by fusing FKBP to the PM cargo Mup1-GFP and FRB to the cytosolic region of the vacuolar adaptor Ssh4. In a strain expressing FRB-Ssh4 and Mup1-GFP-FKBP, FRB-Ssh4 was recruited to the PM upon rapamycin treatment, and Mup1-GFP-FKBP at the PM was consequently endocytosed and degraded during a time course of 6 h, albeit slower than methionine-induced endocytosis (Figure 8A-C). Importantly, this result demonstrates that recruitment of Ssh4, and hence Rsp5, to its target, even at a non-vacuolar location, can result in cargo ubiquitination and degradation.

Given that FRB-Ssh4 was directly recruited to Mup1-GFP-FKBP at the PM upon rapamycin addition, it was not surprising that the FKBP-fused reporter was effectively degraded. However, the temporary localization of FRB-Ssh4 at the PM raised the question of whether other PM proteins lacking FKBP but in proximity to Mup1-FKBP could be degraded in *trans*. To test this issue, I expressed Mup1-Mars in the aforementioned test strain and followed the fate of Mup1-Mars after rapamycin addition (Figure 9A). Interestingly, Mup1-Mars was degraded in *trans* alongside Mup1-GFP-FKBP in 4-6 h (Figure 9B). Importantly, this *trans* degradation was

only observed in the test strain expressing Mup1-GFP-FKBP but not the control strain expressing Mup1-GFP.

Intrigued by these observations, I asked if this FRB-Ssh4-dependent degradation in *trans* was also applicable to other PM proteins. Can1 is a PM arginine permease that localizes to eisosomes, lipid domains of the PM that also contain Mup1 (Douglas et al., 2011; Moharir et al., 2018). Because of its apparent spatial proximity with Mup1, Can1 seemed to be a logical possibility for testing the *trans* interaction. Remarkably, Can1-Mars, when expressed in the strain expressing Mup1-GFP-FKBP and FRB-Ssh4, was also co-endocytosed and sorted to the vacuole lumen for degradation in *trans* (Figure 10). However, the expression of Can1-Mars also resulted in a significantly slower endocytosis and sorting of Mup1-GFP-FKBP (~12-22 h), as seen by accumulation of endocytosed Mup1-GFP-FKBP in intracellular puncta. Furthermore, expression of Can1-Mars also resulted in a slow growth phenotype (Figure S4A and B). To extend these observations further, I asked if FRB-Ssh4-dependent degradation could be observed for other GFP-FKBP-tagged PM cargos. To explore this question, I tagged Can1 with GFP-FKBP in a strain expressing FRB-Ssh4. Can1-GFP-FKBP was efficiently degraded within 1 h of rapamycin treatment (Figure 11A and B). However, neither Can1-Mars nor Mup1-Mars was endocytosed and sorted in *trans* with Can1-GFP-FKBP upon rapamycin treatment (Figure 12A and B). Notably, a slow growth phenotype was observed in all strains expressing Can1-Mars (Figure S4A and C). In summary, rapamycin-induced recruitment of FRB-Ssh4 to the PM results in sorting and degradation of both Mup1-Mars and Can1-Mars in *trans* with Mup1-GFP-FKBP (with slow rapamycin-induced endocytosis ~6 h) but not Can1-GFP-FKBP (with fast rapamycin-induced endocytosis ~1 h; Table 1). Ssh4-dependent *trans* sorting at the PM is significantly

slower and likely requires extended exposure time and close proximity to mediate successful ubiquitination of proximal cargos in *trans* for cargo sorting.

Discussion

Sequential layers of protein surveillance constantly monitor the quality and quantity of membrane proteins in the endocytic system (Figure 13). At the PM, the ART-Rsp5 network performs this task by regulating ubiquitin-dependent endocytosis of cell surface proteins. Intracellular adaptors of Rsp5, Ear1 and Ssh4, provide a crucial second tier of QC for a broad spectrum of endocytosed cargos that escape upstream monitoring and hence prevent toxic build-up of membrane proteins in aberrant locations (Sardana et al., 2018). Cargo recognition by the Art1 adaptor at the PM is thought to require recognition of a specific sequence motif on the cargo (Guiney et al., 2016).

In order to understand the mechanism of cargo recognition by Ssh4-Rsp5 at the VM, I separated ubiquitination events at the PM from those at the VM by adding the acLL motif to biosynthetically reroute PM-bound proteins to the VM via the AP-3 pathway. This strategy permitted me to specifically study Ssh4-mediated cargo recognition, ubiquitination, and degradation in the vacuole lumen. I affixed an acLL motif to multiple PM proteins with diverse topologies and TMDs. Many of the tested candidates still localized to the PM (Figure S1), suggesting that the accessibility of the acLL motif to the AP-3 adaptor at the Golgi was likely hindered, preventing their packaging into vesicles for vacuolar delivery. Additionally, the presence of a dominant PM sorting signal could have superseded the effect of the acLL motif. Nonetheless, the single-TMD Wsc1 and the 12-TMD Mup1 were successfully rerouted to the vacuole, serving as viable reporters for analysis (Figure 1). Interestingly, both Wsc1-acLL and

Mup1-acLL were constitutively sorted to the vacuole lumen by the Ssh4-Rsp5 complex, suggesting a robust recognition mechanism for aberrant proteins.

To understand the features of Ssh4 important for cargo recognition, I tested mutants of Ssh4 lacking key regions in its cytosolic region, namely the SPRY domain and PY motifs. The PY motifs of adaptors have been previously shown to be required for interaction with Rsp5 E3 ubiquitin ligase (Léon et al., 2008). Not surprisingly, the Ssh4^{PY} mutant completely blocked aberrant protein degradation, likely due to a failure to recruit Rsp5 to the VM. SPRY domains are thought to mediate protein-protein interactions, although their function is not completely understood (Woo et al., 2006). While Ssh4 and Ear1 do not appear to have a direct human homologue, the SPRY domain is a common protein interaction adaptor module in higher eukaryotes, and approximately 45% of human SPRY-containing proteins (total of >100) are E3 ubiquitin ligases (Perfetto et al., 2013). I showed that the SPRY domain of Ssh4 is important for cargo sorting, as swapping it with the SPRY domain of Ear1 did not maintain Ssh4 function despite high conservation between the two adaptors. The tested Ssh4 mutants appeared similar to WT Ssh4 in stability and localization pattern, suggesting a specific defect in cargo recognition. However, without understanding the three-dimensional structure of Ssh4 and the mechanism of protein interaction by the SPRY domain, it is difficult to predict how a domain swap alters the spatial interaction of Ssh4 with its intended cargos. The SPRY domain may allow recognition of specific cargo features, or other cytosolic regions of the adaptor may cooperate with the domain to mediate proper function. It is also possible that the SPRY domain stabilizes cargo recognition to allow proper docking of Rsp5 and ubiquitination of the target lysine residues on the cargo. A detailed mutational analysis of the SPRY domain in the future will likely be useful in better understanding how the domain mediates cargo recognition.

This study also highlights the promiscuity of the Ssh4-Rsp5 E3 ubiquitin ligase complex in selecting the lysine residue on the cargo to ubiquitinate. I found that Ssh4-Rsp5 can modify several accessible lysine residues positioned within a "ubiquitination zone" in the cytosolic tail, presumably restricted by the structural constraints of the association of Ssh4-Rsp5 with the membrane and the cargo. Mutating any single lysine to arginine did not block degradation if other cytosolic lysine residues were present in the regions accessible to the Ssh4-Rsp5 complex. Spatial positioning is therefore probably a key factor in determining accessibility, as the lysine residue must be near enough to Ssh4-Rsp5 as well as oriented correctly to allow access for ubiquitination. This somewhat promiscuous but fail-safe mechanism allows the complex to degrade a diverse array of cargos and prevents aberrant accumulation on the membrane of the terminal destination of the endocytic pathway. However, mechanisms also exist to prevent non-specific and constitutive degradation of resident VM proteins by Ssh4-Rsp5. Masking of the cytosolic lysine residues by structural fold or complex formation as well as fewer available lysine residues in the ubiquitination zone of Ssh4-Rsp5 are likely some of the strategies employed to prevent resident VM protein degradation. Indeed, work from the Emr Lab has shown that introduction of a single lysine residue to a structurally flexible cytosolic tail of an otherwise stable VM protein is sufficient to cause constitutive degradation of the VM protein, suggesting that accessible lysine residues are a key recognition signal for Ssh4-Rsp5 (Sardana et al., 2018).

This promiscuous mode of target selection prompted me to ask if placement of Ssh4 on a membrane early in the endocytic or biosynthetic pathway may be detrimental to cellular fitness by causing non-specific protein degradation. While my attempts to redirect Ssh4 to the ER (by fusion of the KKxx motif) or to the PM (by fusion of the PM-targeting region of Rcr1) by

creating chimeric proteins did not work, I successfully recruited Ssh4 to the PM by utilizing the specific interaction between FKBP and FRB modules (Inobe and Nukina, 2016). By fusing the cytosolic region of Ssh4 to FRB, I could recruit it to a PM protein fused to GFP-FKBP, specifically in response to rapamycin addition. Fusion of GFP allowed me to monitor the fate of the PM cargo upon Ssh4 recruitment. Using this strategy, I performed a proof-of-concept experiment that demonstrated that Ssh4 can recruit Rsp5 to target cargos for degradation even at the PM. The degradation kinetics after rapamycin addition were variable for the two cargos I tested (4-6 h for Mup1-GFP-FKBP and 1 h for Can1-GFP-FKBP), likely due to differences in accessibility of the FRB-FKBP interaction in the fusion proteins. I next asked if recruitment of FRB-Ssh4 to the PM could induce non-specific degradation of other proximal PM proteins not tagged with FKBP. My analysis with the two cargos gave different results. The combination of the primary cargo Mup1-GFP-FKBP with the secondary cargos Mup1-Mars or Can1-Mars resulted in the FRB-Ssh4-mediated degradation of both primary and secondary cargos, while the combination of Can1-GFP-FKBP with Mup1-Mars or Can1-Mars only resulted in the degradation of the primary cargo. The main difference between the two was a considerably slower rate of endocytosis and vacuolar sorting for Mup1-GFP-FKBP (Table 1). This observation suggests that the longer exposure time of FRB-Ssh4 to the secondary cargos when recruited to the PM via Mup1-GFP-FKBP, as opposed to Can1-GFP-FKBP, likely allows the *trans* degradation of the secondary cargos. Cargo accessibility is probably also dictated significantly by spatial proximity: both Can1 and Mup1 are eisosome-resident proteins in the PM, allowing extended access of Ssh4-Rsp5 to these cargos. Additionally, the spatial orientation of the cargos and their available cytosolic lysine residues relative to the FRB-tethered Ssh4-Rsp5 in

trans may be severely restricted in different combinations, although this aspect could not be measured.

Finally, non-specific degradation of many PM cargos would also predict an impairment of cellular homoeostasis and decreased cell viability. However, I did not observe a detrimental effect to the fitness of the cells carrying the FRB-FKBP system upon rapamycin-induced recruitment of FRB-Ssh4 to the PM. Intriguingly, I noticed a slow growth phenotype in cells expressing Can1-Mars (Figure S4); however, the basis of this toxicity was independent of Ssh4-mediated degradation. The absence of such a cellular response implies that Ssh4-Rsp5 is not widely and randomly targeting other resident PM proteins for degradation. I speculate that the close spatial proximity and lysine orientation for Ssh4-Rsp5 are critical determinants in limiting the scope of the analysis of non-specific degradation using the FRB-FKBP system. Future analysis using alternative strategies to target Ssh4 will be required to further test these ideas. However, my analysis also indicates that although the fail-safe recognition mechanism employed by Ssh4-Rsp5 at the VM may appear promiscuous, its function may be regulated by the availability and spatial accessibility of the cargo to the catalytic site of Rsp5.

Materials and Methods

Yeast strains and growth conditions

All yeast strains, detailed in Table S1, were constructed using standard transformation techniques (Gietz and Woods, 2002). Strains transformed with centromeric plasmids were grown at 26°C in synthetic media lacking uracil, leucine, and/or tryptophan, as indicated, for plasmid maintenance. Experiments involving the endocytosis of the methionine transporter Mup1 were performed in synthetic media also deficient for methionine. At the outset of experiments utilizing

the FRB-FKBP system, rapamycin was added to a final concentration of 1 μg/ml to mid-log phase cultures grown in appropriate synthetic media.

For yeast dilution spot assays, mid-log phase cultures were grown at 26°C in synthetic complete or selective media. Cells were diluted to 0.3 OD_{600} in 200 μl water, and 10-fold serial dilutions were spotted on the indicated growth media and incubated at 26°C for 2-3 d.

Plasmids and cloning

All plasmids, detailed in Table S2, were constructed using standard molecular cloning techniques (Celie et al., 2016). PCR was performed using Phusion DNA polymerase and associated reagents purchased from Thermo Fisher Scientific. Cloning was accomplished with restriction enzymes purchased from New England Biolabs.

Fluorescence microscopy

Yeast cells were grown to mid-log phase in appropriate synthetic media, and 0.5 OD_{600} equivalent of cells was harvested and washed with water prior to imaging. Microscopy was performed with a DeltaVision Elite system (GE Healthcare Life Sciences) equipped with an Olympus IX-71 inverted microscope, DV Elite complementary metal-oxide semiconductor camera, a 100x/1.4 NA oil objective, and a DV Light SSI 7 Color illumination system with Live Cell Speed Option with DV Elite filter sets (FITC channel for GFP and mCherry channel for mCherry). Images were captured and deconvolved (conservative, four cycles) with the accompanying DeltaVision software softWoRx 6.5.2 (Applied Precision). Images were similarly adjusted for brightness and contrast within a single figure panel, and each image represents a

single focal plane. Images were processed in ImageJ and assembled in Microsoft PowerPoint and Adobe Illustrator CC 2018.

Protein extraction and western blotting

Yeast cells were grown to mid-log phase in appropriate synthetic media, and 5-7 OD_{600} equivalent of cells was harvested and incubated in 10% TCA on ice for 1 h. The cells were washed with acetone and lysed by beating with glass beads in 70 µl of boiling buffer (50 mM Tris-HCl, pH 7.5, 8 M urea, 2% SDS, and 1 mM EDTA) for 5 min at room temperature. Following incubation at 42°C for 5 min, 70 µl of 2x urea sample buffer (150 mM Tris-HCl, pH 6.8, 8 M urea, 8% SDS, 24% glycerol, 100 mM DTT, and bromophenol blue) was added. Samples were vortexed for 5 min at room temperature, incubated at 42°C for 10 min, and centrifuged for 2 min at 21,000 *g* at room temperature to collect the supernatant. 0.5-1.0 OD_{600} equivalent was loaded per lane onto a 10% SDS-polyacrylamide gel and resolved with a constant current of 25 mA. Wet transfer to nitrocellulose membrane (0.45 µm; GE Healthcare) was carried out at 4°C in transfer buffer (25 mM Tris, 192 mM glycine, 20% vol/vol methanol, and 0.006% SDS) for 2 h at 100 V or overnight at 25 V. Membranes were blocked with 5% fat-free milk in 1x TBST (20 mM Tris-HCl, pH 7.5, 150 mM NaCl, and 0.05% Tween-20) and blotted with primary antibodies for 2 h at room temperature or overnight at 4°C. They were then washed thrice with 1x TBST for 10 min each time, incubated with secondary antibodies diluted in 1x TBST for 1 h at room temperature, and again washed thrice with 1x TBST. Membranes were scanned with an Odyssey CLx imaging system and analyzed with Image Studio Lite 5.2.5 (LI-COR Biosciences). Images were assembled in Microsoft PowerPoint and Adobe Illustrator CC 2018.

The following antibodies and dilutions were used: rabbit polyclonal anti-GFP (1:5,000; TP401; Torrey Pines Biolabs), mouse monoclonal anti-PGK (1:5,000; 22C5D8; Molecular Probes), 800CW goat anti-rabbit (1:10,000; 926-32211; LI-COR Biosciences), and 680LT goat anti-mouse (1:10,000; 926-68021; LI-COR Biosciences).

Acknowledgements

I am deeply grateful to Prof. Scott Emr for taking a chance on me early in my college career and providing me with an excellent learning environment that has proved both formative and enjoyable. I am indebted to Dr. Richa Sardana, who has wisely and patiently mentored me every step of the way. Her feedback on this thesis was invaluable, but her counsel on how to perform good science and how to view the natural world with curiosity and wonder will remain with me for a lifetime. Many thanks to the rest of the Emr Lab for helpful discussions and daily encouragement. Thank you, my family and friends, for your love and support that I will never be able to repay.

References

Belgareh-Touzé, N., S. Léon, Z. Erpapazoglou, M. Stawiecka-Mirota, D. Urban-Grimal, and R. Haguenauer-Tsapis. 2008. Versatile role of the yeast ubiquitin ligase Rsp5p in intracellular trafficking. *Biochem. Soc. Trans.* 36:791–796. doi:10.1042/BST0360791.

Benghezal, M., G.O. Wasteneys, and D.A. Jones. 2000. The C-Terminal Dilysine Motif Confers Endoplasmic Reticulum Localization to Type I Membrane Proteins in Plants. *Plant Cell*. 12:1179–1201. doi:10.1105/tpc.12.7.1179.

Berner, N., K.-R. Reutter, and D.H. Wolf. 2018. Protein Quality Control of the Endoplasmic Reticulum and Ubiquitin-Proteasome-Triggered Degradation of Aberrant Proteins: Yeast Pioneers the Path. *Annu. Rev. Biochem.* 87:751–782. doi:10.1146/annurev-biochem-062917-012749.

Celie, P.H.N., A.H.A. Parret, and A. Perrakis. 2016. Recombinant cloning strategies for protein expression. *Curr. Opin. Struct. Biol.* 38:145–154. doi:10.1016/j.sbi.2016.06.010.

Cowles, C.R., G. Odorizzi, G.S. Payne, and S.D. Emr. 1997. The AP-3 Adaptor Complex Is Essential for Cargo-Selective Transport to the Yeast Vacuole. *Cell*. 91:109–118. doi:10.1016/S0092-8674(01)80013-1.

D'Cruz, A.A., J.J. Babon, R.S. Norton, N.A. Nicola, and S.E. Nicholson. 2013. Structure and function of the SPRY/B30.2 domain proteins involved in innate immunity. *Protein Sci.* 22:1–10. doi:10.1002/pro.2185.

Darsow, T., C.G. Burd, and S.D. Emr. 1998. Acidic di-leucine motif essential for AP-3-dependent sorting and restriction of the functional specificity of the Vam3p vacuolar t-SNARE. *J. Cell Biol.* 142:913–922. doi:10.1083/jcb.142.4.913.

Douglas, L.M., H.X. Wang, L. Li, and J.B. Konopka. 2011. Membrane Compartment Occupied by Can1 (MCC) and Eisosome Subdomains of the Fungal Plasma Membrane. *Membranes (Basel).* 1:394–411. doi:10.3390/membranes1040394.

Gaynor, E.C., S. te Heesen, T.R. Graham, M. Aebi, and S.D. Emr. 1994. Signal-mediated Retrieval of a Membrane Protein from the Golgi to the ER in Yeast. *J. Cell Biol.* 127:653–665. doi:10.1083/jcb.127.3.653.

Gietz, R.D., and R.A. Woods. 2002. Transformation of yeast by lithium acetate/single-stranded carrier DNA/polyethylene glycol method. *Methods Enzymol.* 350:87–96. doi:10.1016/S0076-6879(02)50957-5.

Guiney, E.L., T. Klecker, and S.D. Emr. 2016. Identification of the endocytic sorting signal recognized by the Art1-Rsp5 ubiquitin ligase complex. *Mol. Biol. Cell*. 27:4043–4054. doi:10.1091/mbc.e16-08-0570.

Henne, W.M., H. Stenmark, and S.D. Emr. 2013. Molecular Mechanisms of the Membrane Sculpting ESCRT Pathway. *Cold Spring Harb. Perspect. Biol.* 1–12. doi:10.1101/cshperspect.a016766.

Inobe, T., and N. Nukina. 2016. Rapamycin-induced oligomer formation system of FRB–FKBP fusion proteins. *J. Biosci. Bioeng.* 122:40–46. doi:10.1016/j.jbiosc.2015.12.004.

Isnard, A.-D., D. Thomas, and Y. Surdin-Kerjan. 1996. The study of methionine uptake in Saccharomyces cerevisiae reveals a new family of amino acid permeases. *J. Mol. Biol.* 262:473–484. doi:10.1006/jmbi.1996.0529.

Léon, S., Z. Erpapazoglou, and R. Haguenauer-Tsapis. 2008. Ear1p and Ssh4p Are New Adaptors of the Ubiquitin Ligase Rsp5p for Cargo Ubiquitylation and Sorting at Multivesicular Bodies. *Mol. Biol. Cell*. 19:2379–2388. doi:10.1091/mbc.E08-01-0068.

Léon, S., and R. Haguenauer-Tsapis. 2009. Ubiquitin ligase adaptors: Regulators of ubiquitylation and endocytosis of plasma membrane proteins. *Exp. Cell Res.* 315:1574–1583. doi:10.1016/j.yexcr.2008.11.014.

Lin, C.H., J.A. MacGurn, T. Chu, C.J. Stefan, and S.D. Emr. 2008. Arrestin-Related Ubiquitin-Ligase Adaptors Regulate Endocytosis and Protein Turnover at the Cell Surface. *Cell*. 135:714–725. doi:10.1016/j.cell.2008.09.025.

MacGurn, J.A., P.-C. Hsu, and S.D. Emr. 2012. Ubiquitin and Membrane Protein Turnover: From Cradle to Grave. *Annu. Rev. Biochem.* 81:231–259. doi:10.1146/annurev-biochem-060210-093619.

Moharir, A., L. Gay, D. Appadurai, J. Keener, and M. Babst. 2018. Eisosomes are metabolically regulated storage compartments for APC-type nutrient transporters. *Mol. Biol. Cell*. 29:2113–2127. doi:10.1091/mbc.E17-11-0691.

Perfetto, L., P.F. Gherardini, N.E. Davey, F. Diella, M. Helmer-Citterich, and G. Cesareni. 2013. Exploring the diversity of SPRY/B30.2-mediated interactions. *Trends Biochem. Sci.* 38:38–46. doi:10.1016/j.tibs.2012.10.001.

Philip, B., and D.E. Levin. 2001. Wsc1 and Mid2 Are Cell Surface Sensors for Cell Wall Integrity Signaling That Act through Rom2, a Guanine Nucleotide Exchange Factor for Rho1. *Mol. Cell. Biol.* 21:271–280. doi:10.1128/MCB.21.1.271.

Piper, R.C., I. Dikic, and G.L. Lukacs. 2014. Ubiquitin-Dependent Sorting in Endocytosis. *Cold Spring Harb. Perspect. Biol.* 1–21. doi:10.1101/cshperspect.a016808.

Putyrski, M., and C. Schultz. 2012. Protein translocation as a tool: The current rapamycin story. *FEBS Lett.* 586:2097–2105. doi:10.1016/j.febslet.2012.04.061.

Robinson, J.S., D.J. Klionsky, L.M. Banta, and S.D. Emr. 1988. Protein sorting in Saccharomyces cerevisiae: isolation of mutants defective in the delivery and processing of multiple vacuolar hydrolases. *Mol. Cell. Biol.* 8:4936–4948. doi:10.1128/mcb.8.11.4936.

Sardana, R., L. Zhu, and S.D. Emr. 2018. Rsp5 Ubiquitin ligase-mediated quality control system clears membrane proteins mistargeted to the vacuole membrane. *J. Cell Biol.* 218:234–250. doi:10.1083/jcb.201806094.

Vowels, J.J., and G.S. Payne. 1998. A dileucine-like sorting signal directs transport into an AP-3-dependent, clathrin-independent pathway to the yeast vacuole. *EMBO J.* 17:2482–2493. doi:10.1093/emboj/17.9.2482.

Woo, J.-S., J.-H. Imm, C.-K. Min, K.-J. Kim, S.-S. Cha, and B.-H. Oh. 2006. Structural and functional insights into the B30.2/SPRY domain. *EMBO J.* 25:1353–1363. doi:10.1038/sj.emboj.7600994.

Zhao, Y., J.A. MacGurn, M. Liu, and S. Emr. 2013. The ART-Rsp5 ubiquitin ligase network comprises a plasma membrane quality control system that protects yeast cells from proteotoxic stress. *Elife*. 1–18. doi:10.7554/eLife.00459.

Zhu, L., J.R. Jorgensen, M. Li, Y.-S. Chuang, and S.D. Emr. 2017. ESCRTs function directly on the lysosome membrane to downregulate ubiquitinated lysosomal membrane proteins. *Elife*. 1–20. doi:10.7554/eLife.26403.

Figures

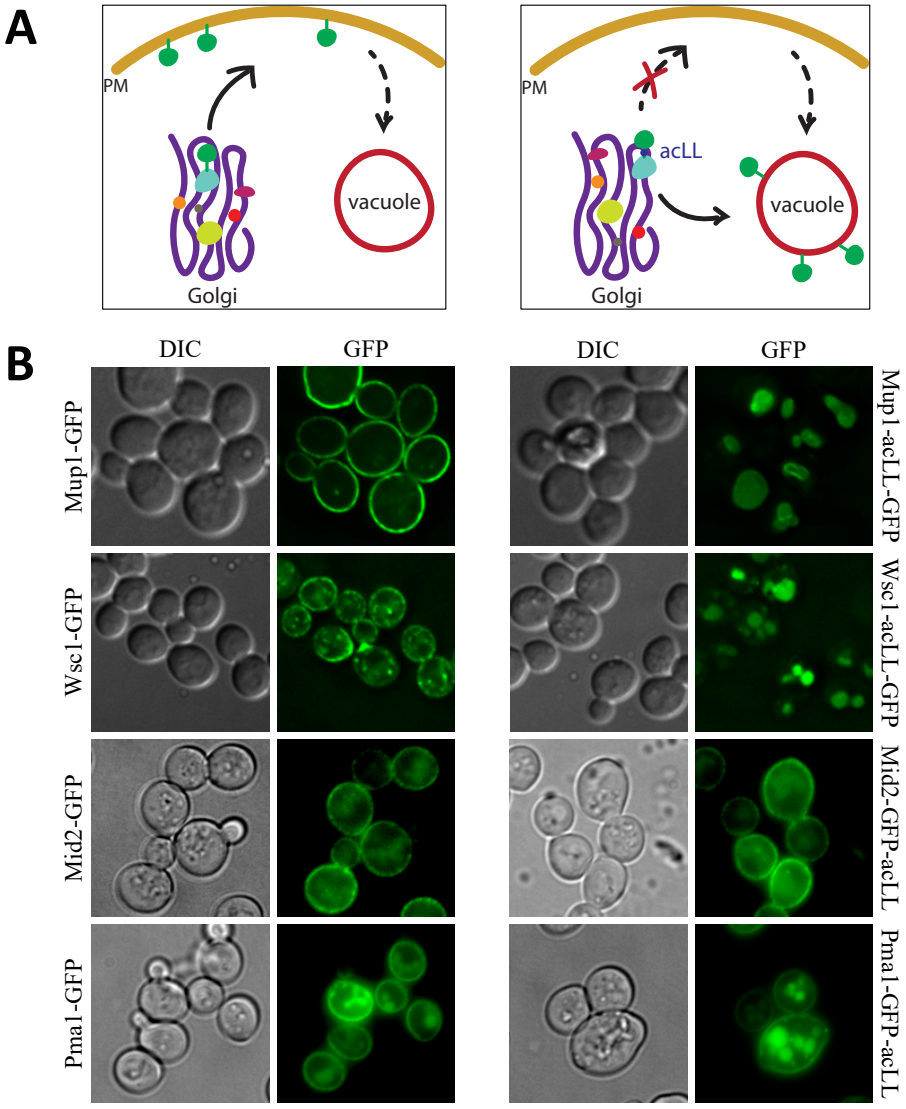

Figure 1. Adding an acLL motif misdirects some but not all PM proteins to the vacuole. (A) Strategy to biosynthetically misdirect GFP-tagged PM proteins to the vacuole by fusing an acLL motif recognized by the AP-3 adaptor. **(B)** Fluorescence microscopy of cells expressing PM proteins tagged with an acLL motif. Mup1 and Wsc1 were successfully mistargeted to the vacuole with this strategy, while the acLL motif had no effect on the localization of Mid1 and Pma1. See Figure S1 for additional acLL-tagged GFP reporters that were tested.

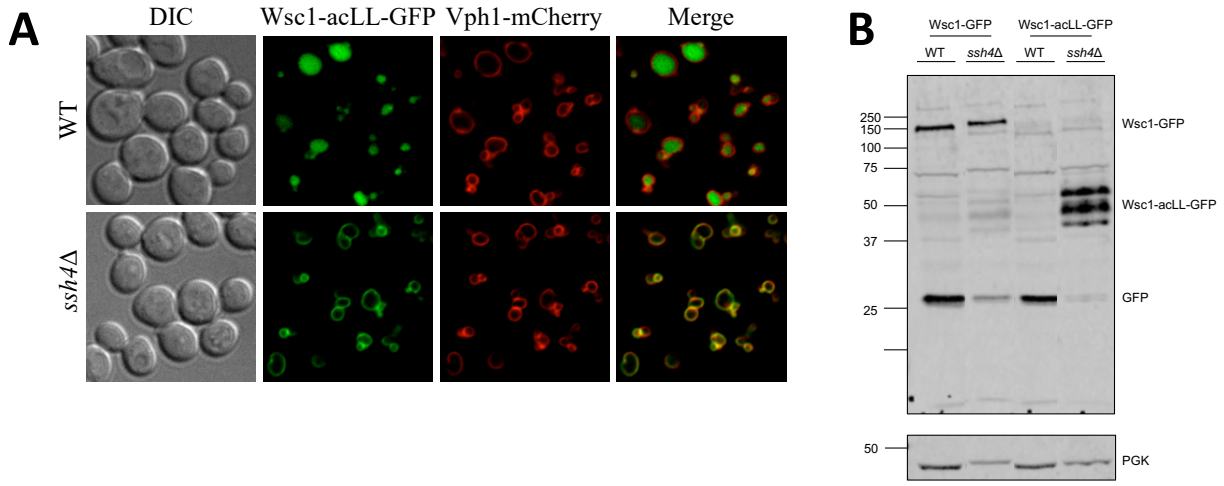

Figure 2. Ssh4 is required for recognition and degradation of aberrant proteins at the VM. **(A)** Fluorescence microscopy of WT or *ssh4*Δ cells expressing Wsc1-acLL-GFP. The reporter was localized to the vacuole lumen in WT cells at steady state and blocked on the VM in *ssh4*Δ cells. Vph1-mCherry was used as a VM marker. **(B)** Western blot of whole cell extracts prepared from WT or *ssh4*Δ cells expressing Wsc1-GFP or Wsc1-acLL-GFP. *ssh4*Δ cells expressing Wsc1-GFP showed a reduction in free GFP relative to the WT control. The N-terminal region of Wsc1-acLL-GFP in *ssh4*Δ cells was clipped by luminal proteases, producing multiple processed bands, but the reporter continued to accumulate on the VM, as shown in (A), instead of being sorted to the lumen for degradation, leading to a reduction in free GFP.

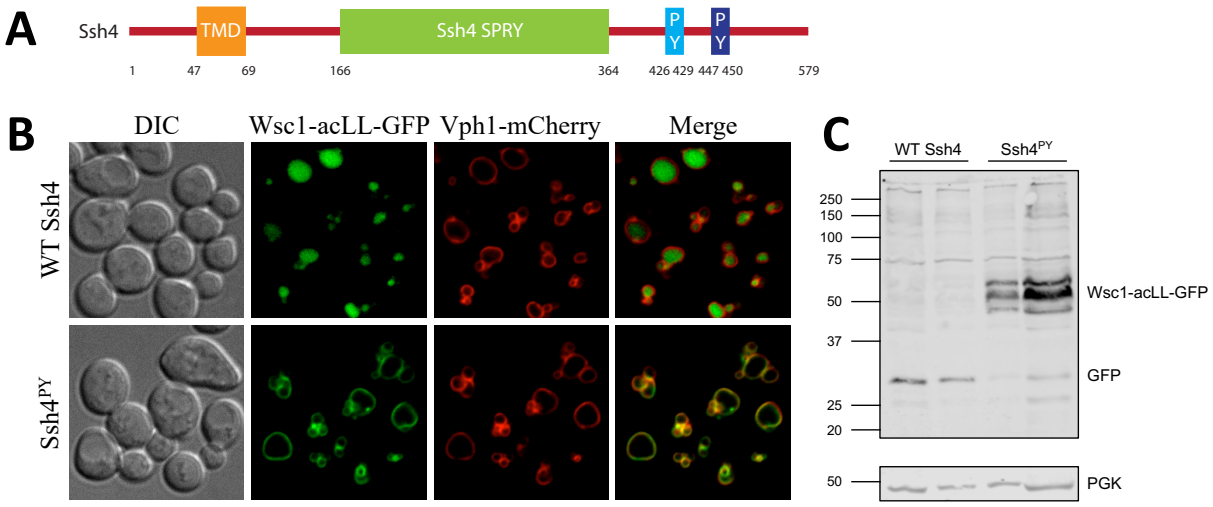

Figure 3. PY motifs of Ssh4 are required for cargo sorting at the VM. (A) Features of Ssh4, including the TMD, SPRY domain, and PY motifs. Numbers indicate aa positions. **(B)** Fluorescence microscopy of *ssh4*Δ cells expressing Wsc1-acLL-GFP and either WT Ssh4 or Ssh4^{PY} mutant. The cargo was sorted to the vacuole lumen when WT Ssh4 was present, but the cargo was blocked on the VM when the PY motifs of Ssh4 were mutated. **(C)** Western blot of whole cell extracts prepared from *ssh4*Δ cells expressing Wsc1-acLL-GFP and either WT Ssh4 or Ssh4^{PY} mutant. Cells expressing WT Ssh4 accumulated a free GFP band indicative of vacuolar degradation, while cells expressing Ssh4^{PY} mutant exhibited an accumulation of processed Wsc1-acLL-GFP resulting from a VM block.

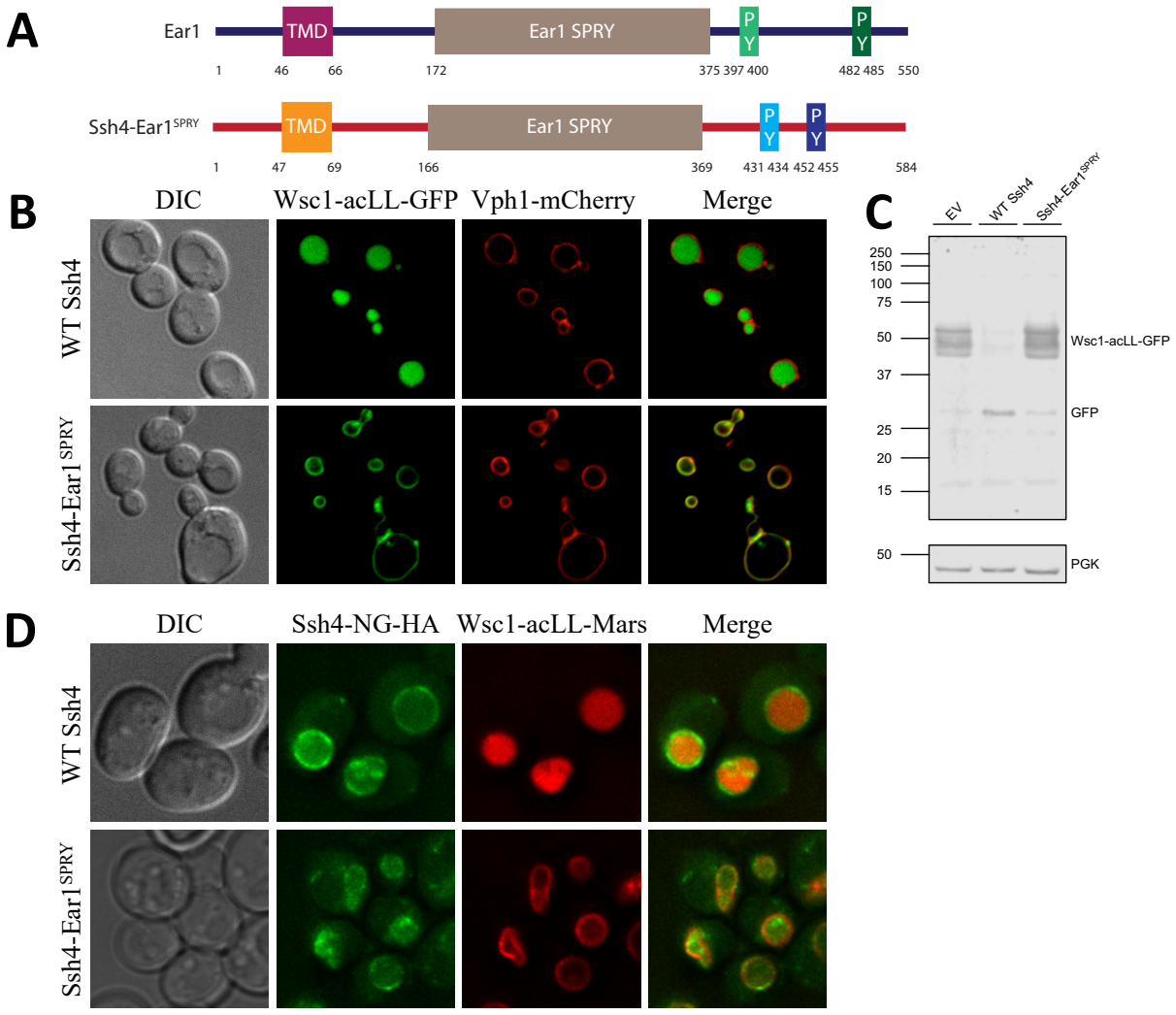

Figure 4. SPRY domain of Ssh4 is important for function in cargo sorting. (A) Features of the endosomal adaptor Ear1 and the Ssh4-Ear1^{SPRY} construct. Numbers indicate aa positions. **(B)** Fluorescence microscopy of *ssh4*Δ cells expressing Wsc1-acLL-GFP and either WT Ssh4 or Ssh4-Ear1^{SPRY}. The cargo was sorted to the vacuole lumen when WT Ssh4 was present, but the cargo was blocked on the VM when the SPRY domain of WT Ssh4 was swapped with the SPRY domain of Ear1. **(C)** Western blot of whole cell extracts prepared from *ssh4*Δ cells expressing Wsc1-acLL-GFP and an empty vector (EV), WT Ssh4, or Ssh4-Ear1^{SPRY}. Only cells expressing WT Ssh4 yielded a significant free GFP band. **(D)** Fluorescence microscopy of *ssh4*Δ cells

expressing Wsc1-acLL-Mars and either WT Ssh4-NG-HA or Ssh4-Ear1^{SPRY}-NG-HA. WT Ssh4 and Ssh4-Ear1^{SPRY} showed similar localization, but the cargo was sorted to the vacuole lumen when WT Ssh4 was present and blocked on the VM when Ssh4-Ear1^{SPRY} was present.

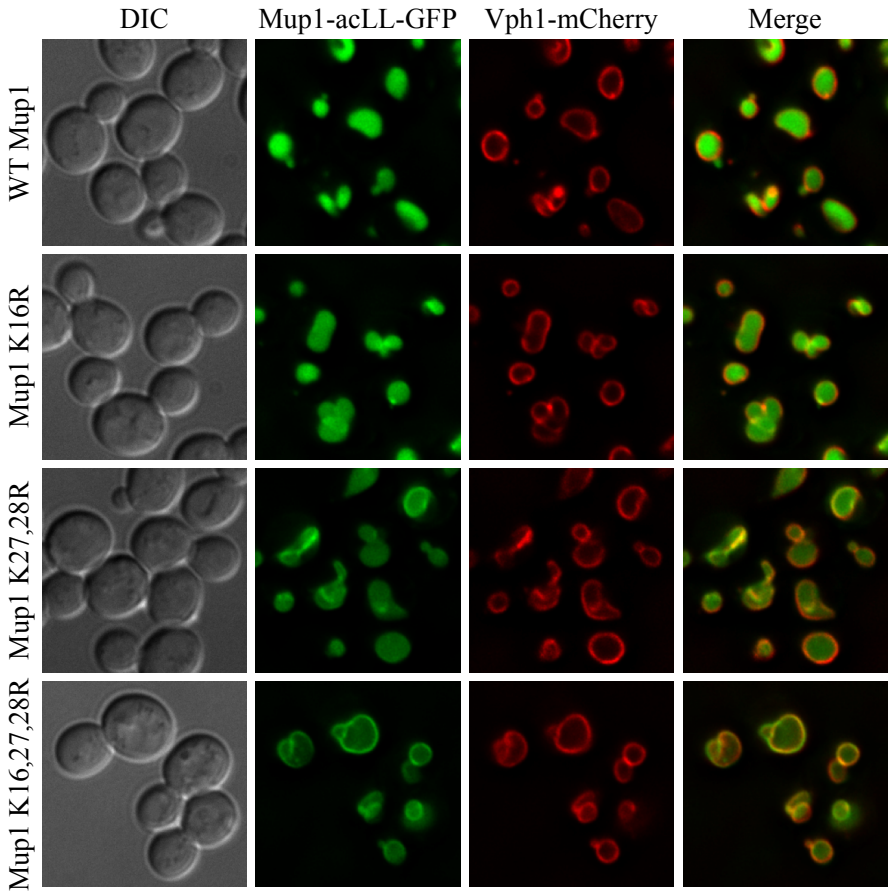

Figure 5. Multiple lysine residues can be recognized by Ssh4-Rsp5 at the VM. Fluorescence microscopy of cells expressing Mup1-acLL-GFP with mutated lysine residues in the cytosolic N-terminal tail. Individual mutation of three lysine residues (K16R, K27R, and K28R) did not block degradation, but combining all three mutations blocked degradation.

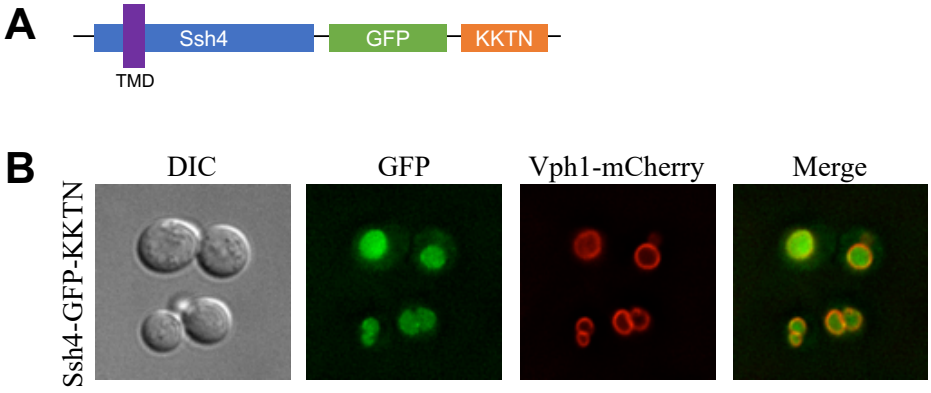

Figure 6. Adding a KKxx motif to Ssh4 fails to mistarget the adaptor to the ER. (A) Features of Ssh4-GFP-KKTN. **(B)** Adding a KKTN motif to Ssh4 did not mistarget it to the ER.

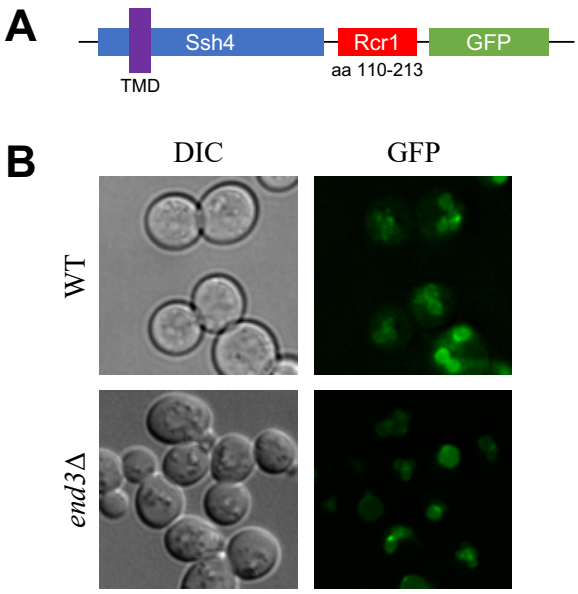

Figure 7. Fusing the Rcr1 C-terminal tail to Ssh4 fails to mistarget the adaptor to the PM. **(A)** Features of Ssh4-Rcr1^{Ctail}-GFP. Amino acids 110-213 of Rcr1 were fused to Ssh4. **(B)** The fusion construct was transformed in a WT strain and an endocytosis-defective *end3*Δ strain. Ssh4 was not mistargeted to the PM in either case, and the absence of PM localization in the *end3*Δ strain suggested that the fusion construct failed to localize to the PM rather than underwent constitutive endocytosis.

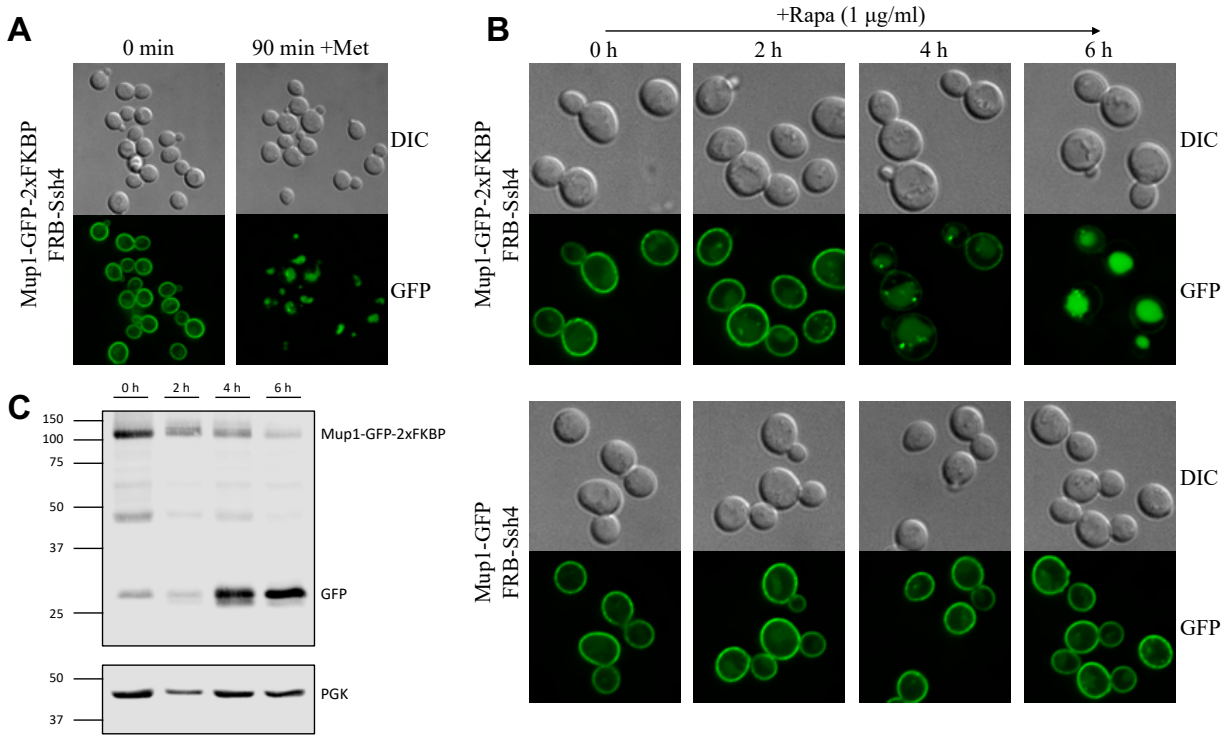

Figure 8. FRB-Ssh4 is mistargeted to the PM upon rapamycin addition and degrades Mup1-GFP-FKBP. (A) Mup1-GFP-FKBP was endocytosed upon methionine (Met; 20 µg/ml) addition (90 min). **(B)** Rapamycin (Rapa; 1 µg/ml) was added to the test strain expressing Mup1-GFP-FKBP and a control strain expressing Mup1-GFP. Both strains also expressed FRB-Ssh4. Only Mup1-GFP-FKBP was endocytosed (4-6 h). **(C)** Western blot of whole cell extracts prepared from cells expressing the test strain. The decrease in full-length Mup1-GFP-FKBP and the appearance of a free GFP band with the progression of time corroborated the microscopy results.

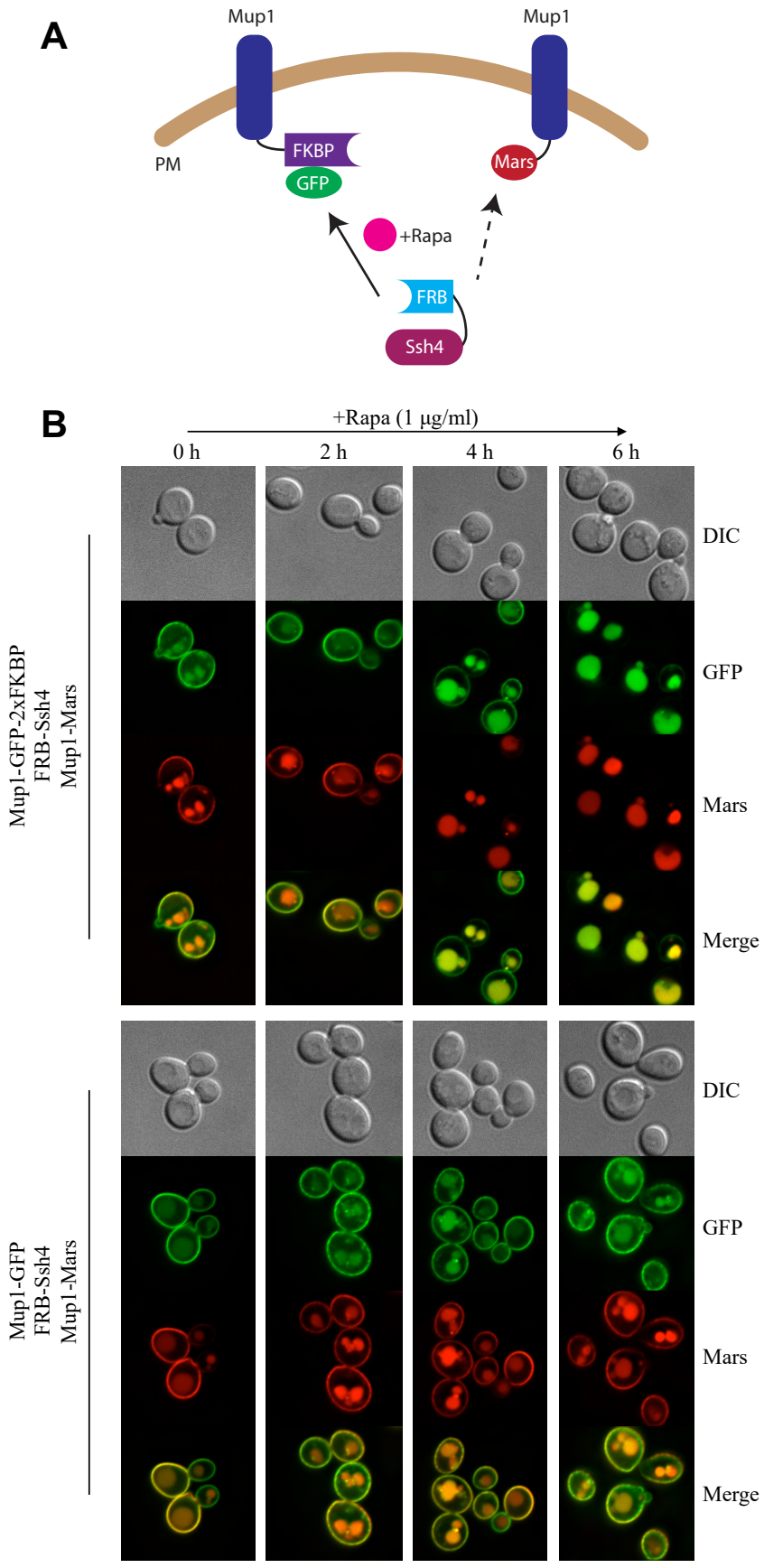
A
Mup1
Mup1
PM
FKBP
GFP
Mars
+Rapa
FRB
Ssh4
B
+Rapa (1 µg/ml)
0 h
2 h
4 h
6 h
Mup1-GFP-2xFKBP
FRB-Ssh4
Mup1-Mars
DIC
GFP
Mars
Merge
Mup1-GFP
FRB-Ssh4
Mup1-Mars
DIC
GFP
Mars
Merge

Figure 9. Recruitment of FRB-Ssh4 upon rapamycin addition to Mup1-GFP-FKBP degrades Mup1-Mars in *trans*. (A) Addition of rapamycin recruits FRB-Ssh4 to Mup1-GFP-FKBP at the PM. FRB-Ssh4 then degrades Mup1-Mars in *trans*. **(B)** Rapamycin (1 μg/ml) was added to the test strain expressing Mup1-GFP-FKBP and a control strain expressing Mup1-GFP. Both strains also expressed FRB-Ssh4 and Mup1-Mars. Mup1-GFP-FKBP and Mup1-Mars were endocytosed in the test strain (4-6 h), while Mup1-GFP and Mup1-Mars remained on the PM in the control strain.

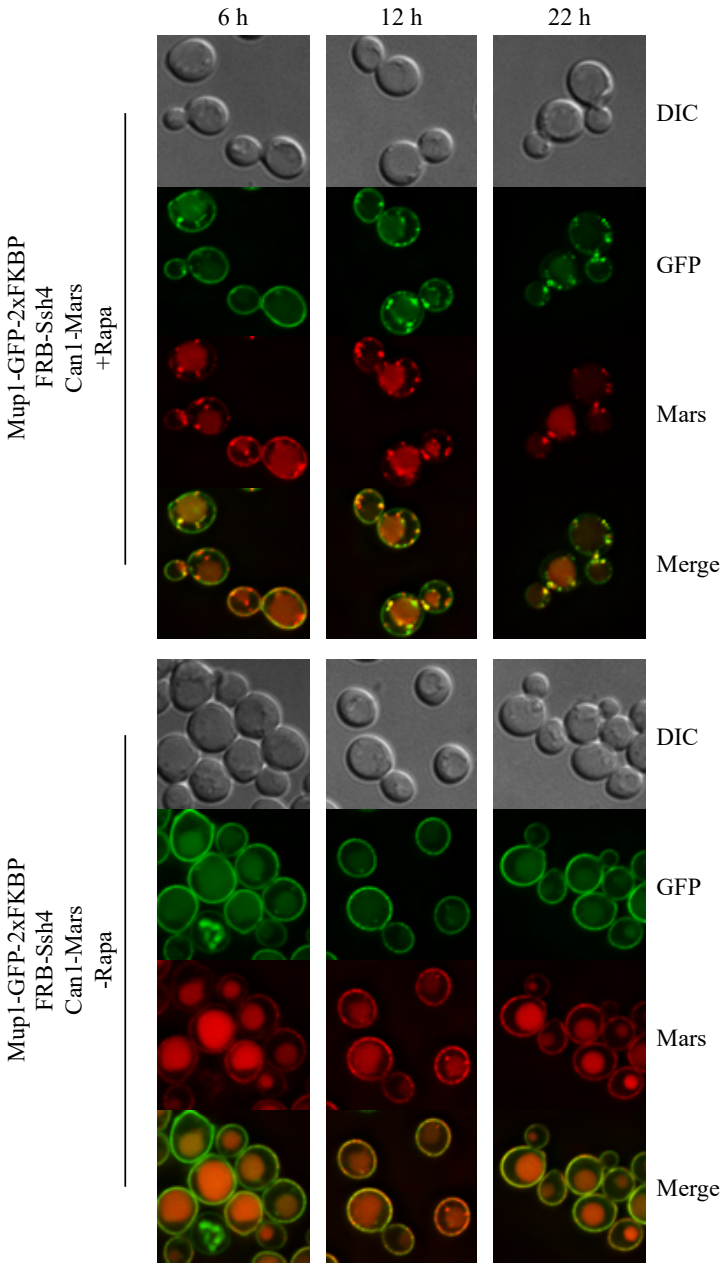

Figure 10. Recruitment of FRB-Ssh4 upon rapamycin addition to Mup1-GFP-FKBP degrades Can1-Mars in *trans*. Addition of rapamycin (1 μg/ml) to a strain expressing Mup1-GFP-FKBP, FRB-Ssh4, and Can1-Mars induced a markedly slower degradation of Mup1-GFP-FKBP compared to the results observed in Figures 8 and 9. Both Mup1-GFP-FKBP and Can1-Mars were gradually degraded over the span of 12-22 h.

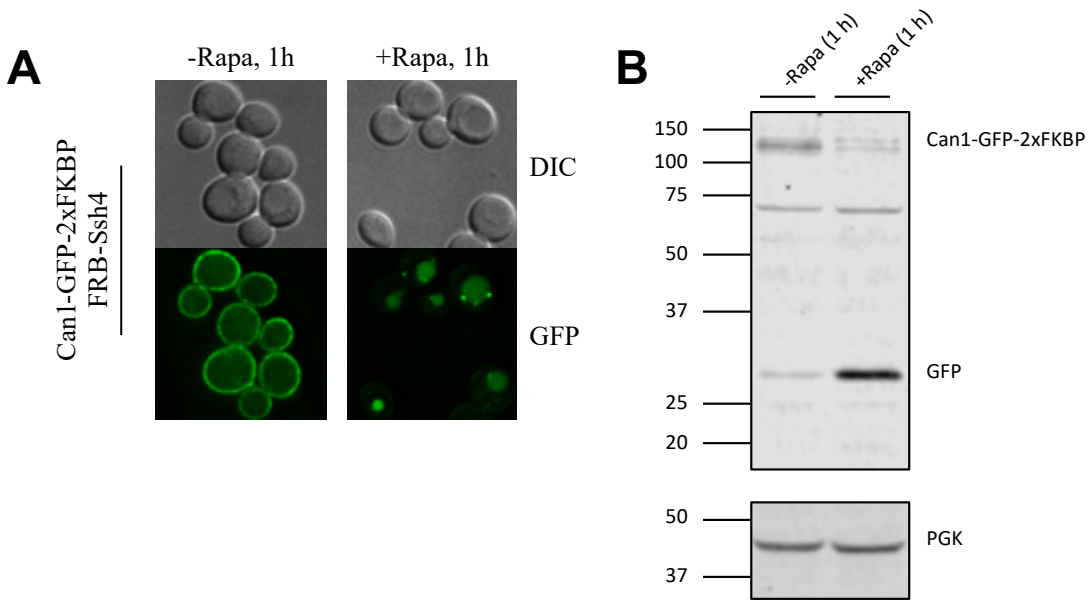

Figure 11. FRB-Ssh4 is mistargeted to the PM upon rapamycin addition and degrades Can1-GFP-FKBP. (A) Can1-GPF-FKBP was endocytosed upon addition of rapamycin (1 µg/ml; 1 h). **(B)** Western blot of whole cell extracts prepared from cells expressing Can1-GFP-FKBP and FRB-Ssh4. Rapamycin-treated cells showed a reduction in full-length Can1-GFP-FKBP and an increase in free GFP.

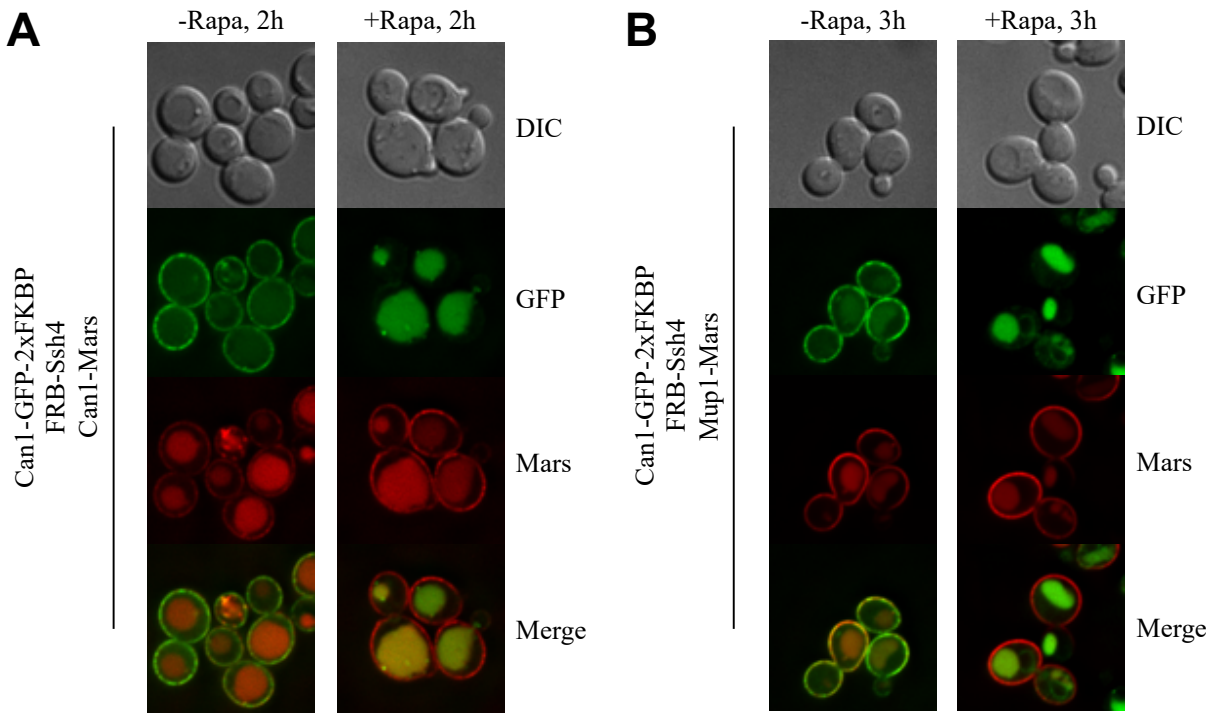

Figure 12. Recruitment of FRB-Ssh4 upon rapamycin addition to Can1-GFP-FKBP does not degrade Can1-Mars or Mup1-Mars in *trans*. (A) Rapamycin-induced degradation of Can1-GFP-FKBP did not result in an accompanying degradation of Can1-Mars in *trans*. Can1-GFP-FKBP was mostly degraded after 1 h of rapamycin (1 μg/ml) treatment. **(B)** Rapamycin-induced degradation of Can1-GFP-FKBP did not result in an accompanying degradation of Mup1-Mars in *trans*. Can1-GFP-FKBP was mostly degraded after 1 h of rapamycin (1 μg/ml) treatment.

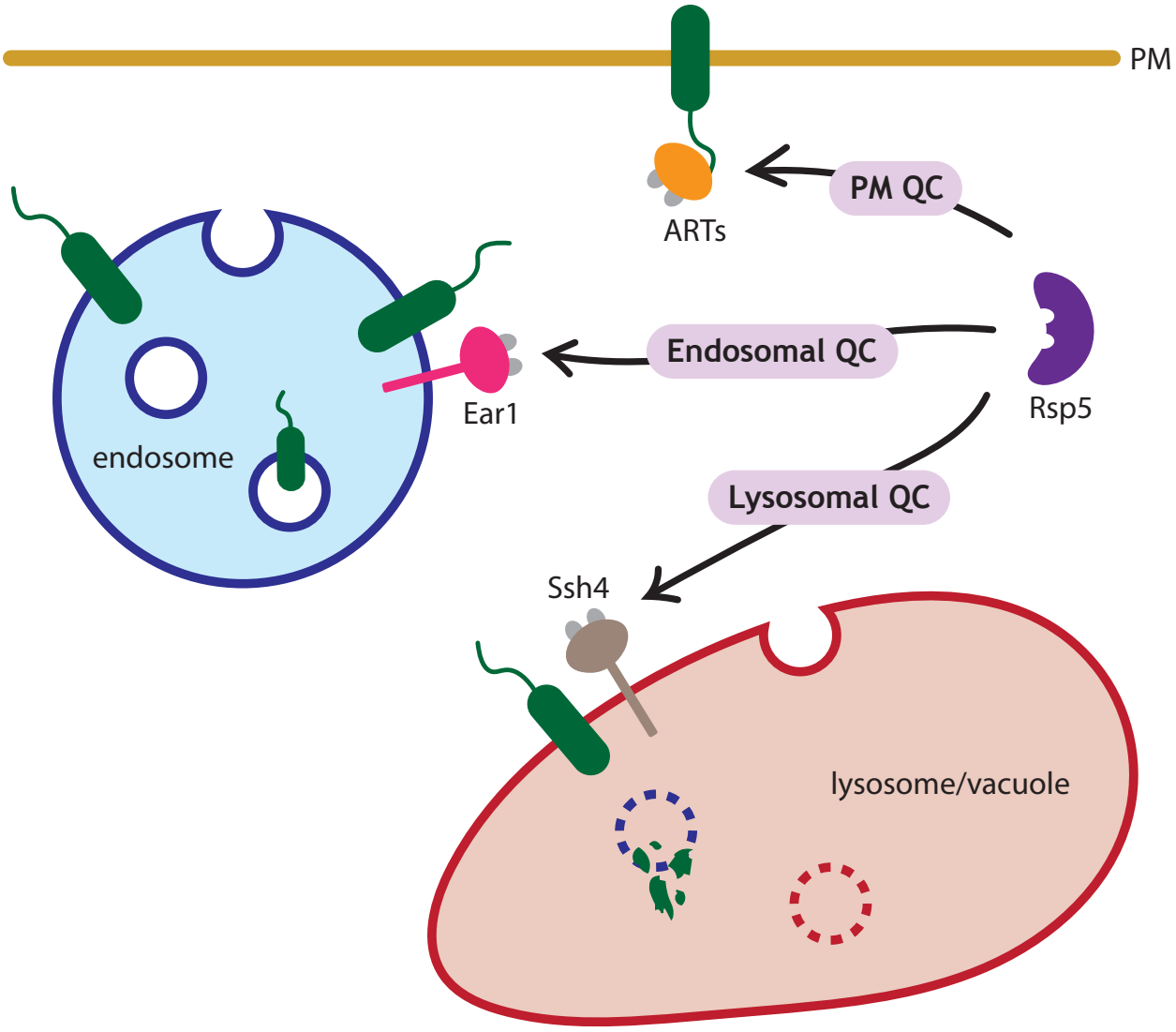

Figure 13. Sequential QC systems monitor membrane proteins in the endocytic pathway. Rsp5 E3 ubiquitin ligase, a key player in the ubiquitination and degradation of endocytic cargos, is recruited to target proteins by specialized adaptors. At the PM, the ART adaptor network facilitates Rsp5-mediated endocytosis of cell surface proteins. Intracellular adaptors Ear1 and Ssh4 regulate additional organelle-specific tiers of QC at the endosome and vacuole, respectively.

x-GFP-FKBP	*y*-Mars	FRB-*z*	Rapa	Sorted?
Mup1	-	Ssh4	+	Yes (4-6 h)
Mup1	Mup1	Ssh4	+	Mup1-GFP-FKBP: Yes (4-6 h) Mup1-Mars: Yes (4-6 h)
Mup1	Can1	Ssh4	+	Mup1-GFP-FKBP: Yes (12-22 h) Can1-Mars: Yes (12-22 h)
Can1	-	Ssh4	+	Yes (1 h)
Can1	Can1	Ssh4	+	Can1-GFP-FKBP: Yes (1 h) Can1-Mars: No
Can1	Mup1	Ssh4	+	Can1-GFP-FKBP: Yes (1 h) Mup1-Mars: No

Table 1. Mup1-Mars and Can1-Mars are degraded in *trans* when FRB-Ssh4 is recruited to Mup1-GFP-FKBP. Summary of the experiments using an FRB-FKBP system to mistarget Ssh4 to the PM. *x* should be read as Mup1 or Can1, *y* should be read as Mup1 or Can1, and *z* should be read as Ssh4. All combinations were treated with rapamycin to determine sorting.

Supplemental Material

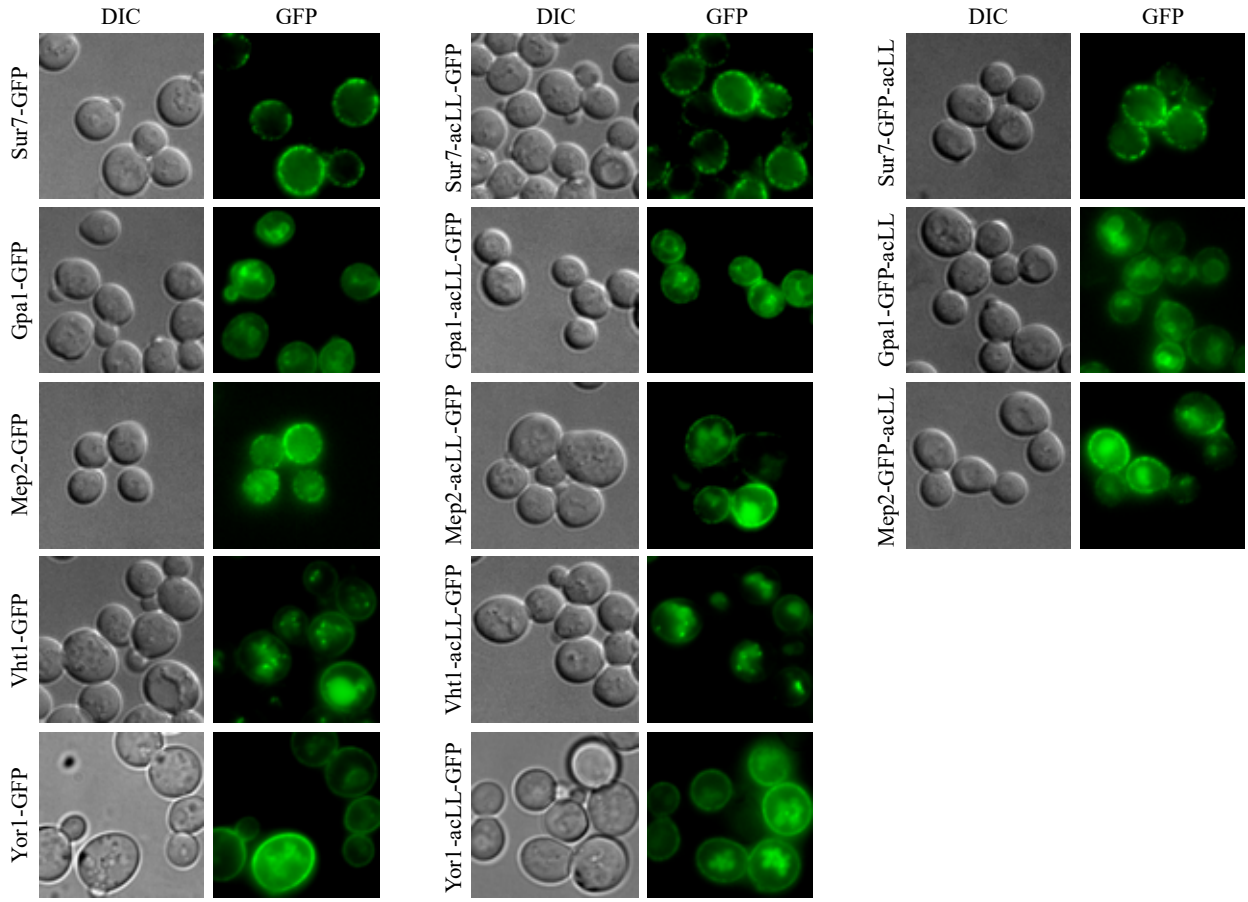

Figure S1. Additional acLL-tagged PM proteins are not mistargeted to the vacuole. The addition of the acLL motif to the indicated PM proteins did not result in their rerouting to the vacuole. The left column shows the localization of the WT proteins. The middle column displays the addition of the acLL motif between the protein and the GFP tag. The right column features the acLL motif placed to the C-terminal side of the GFP tag in an attempt to increase the accessibility of the motif to the AP-3 adaptor.

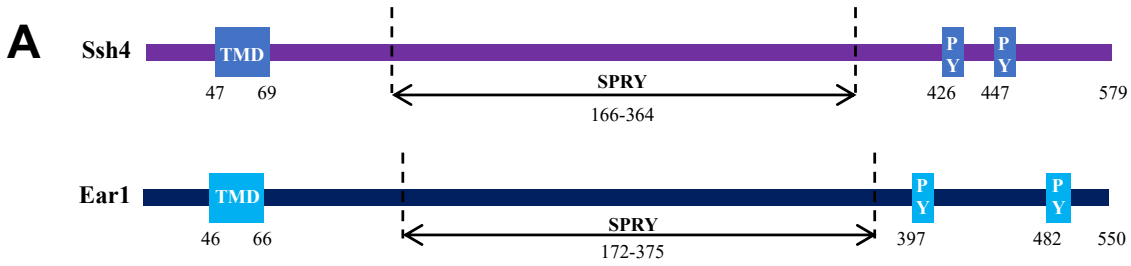

B

Score	Expect	Method	Identities	Positives	Gaps
103 bits(258)	1e-32	Compositional matrix adjust.	63/166(38%)	93/166(56%)	19/166(11%)

```
Ssh4 SPRY  2    QQFIKDRGIQSYFLLPSINDNIDEYGNFLPSFIVQDKLDIQFSKFNKSSSTVMNYPLPHN  61
                +Q+I++ G  ++   P  N ++  +     + IV++K ++ F  +N  +S   N P+P
Ear1 SPRY  11   RQYIQEEGAYAWEFSP--NPDMPNH-----TVIVENKTEVSFLNYNYDASISTNLPIPCI  63

Ssh4 SPRY  62   RKDAVYFEVKIFRHIQKSNS-------IFSIGLTTVPYPYFRVPGMAKYSIAYESTGKLR  114
                 K   Y E KIF      NS       + S GL+T PYPYFR+PG   +SIAY+S G  R
Ear1 SPRY  64   NK-VYYCEFKIFETDGPLNSDENVSKGVISFGLSTQPYPYFRLPGRHHHSIAYDSNGARR  122

Ssh4 SPRY  115  INNPFTAS----TLLPKLEEGDTVGFGYRYKTGTIFITHNGKKLMD  156
                 N+ F  +    TL P+ E+GD VG GYR ++GT+F T NGKKL +
Ear1 SPRY  123  FNDSFKLNEQLRTLFPQCEKGDIVGIGYRSRSGTVFFTRNGKKLNE  168
```

Figure S2. Ssh4 and Ear1 share a similar architecture, including the SPRY domain. (A) Ssh4 and Ear1 each contain a TMD, SPRY domain, and PY motifs. Numbers indicate aa positions. **(B)** The NCBI's Basic Local Alignment Search Tool (BLAST) was used to compare the aa sequences of the SPRY domains of Ssh4 (aa 166-364) and Ear1 (aa 172-375), resulting in 38% identity. BLAST is located at https://blast.ncbi.nlm.nih.gov/Blast.cgi.

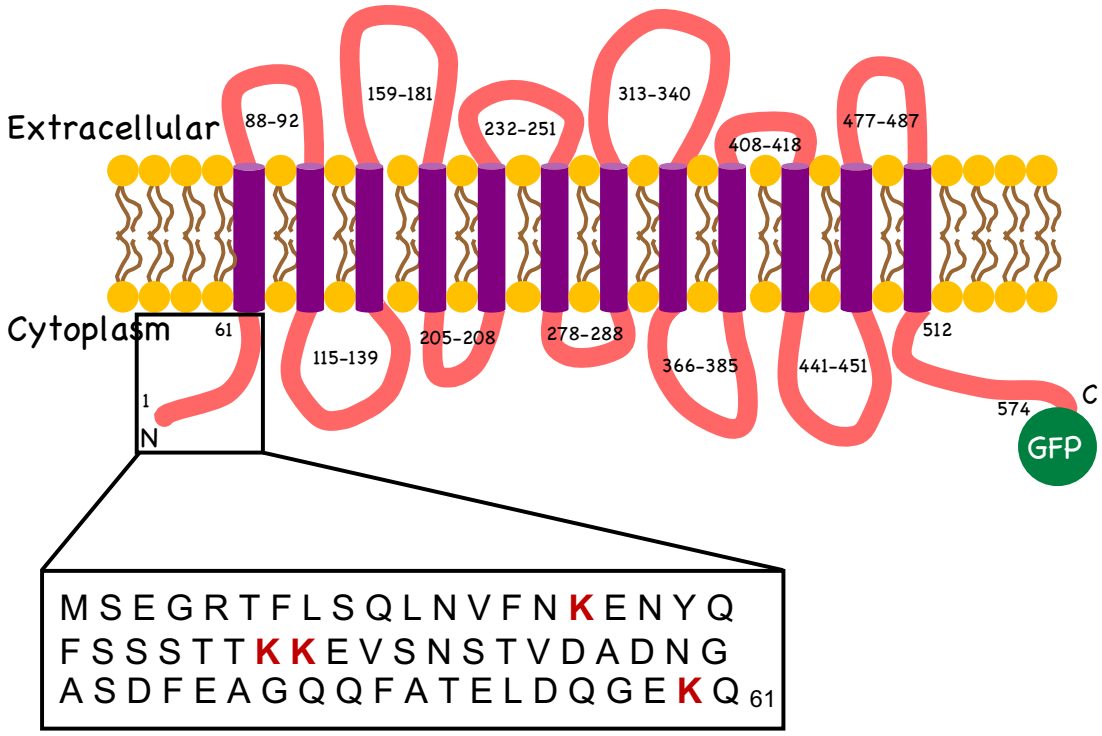

Figure S3. Cytosolic N-terminal tail of Mup1-acLL-GFP contains four lysine residues. The four lysine residues are located at aa positions 16, 27, 28, and 59.

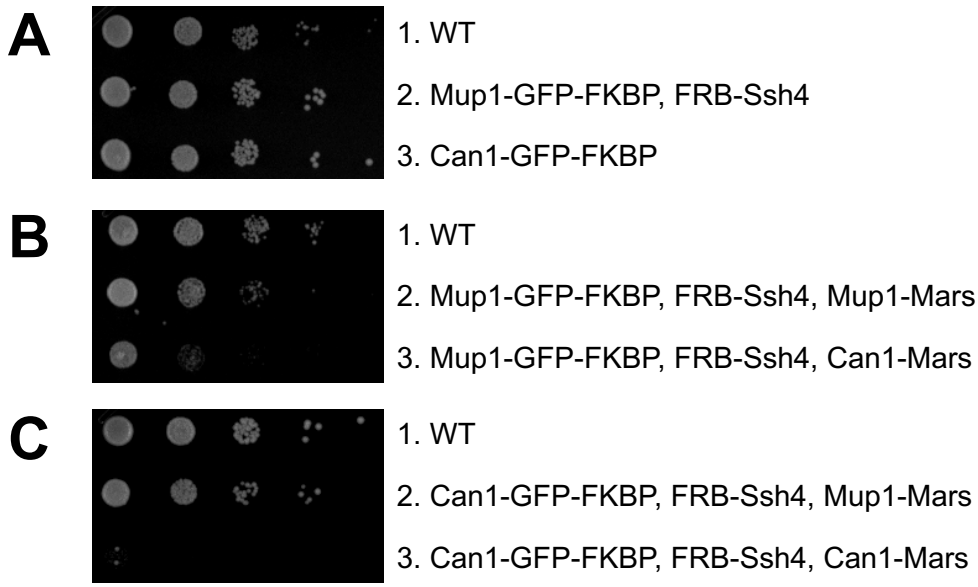

Figure S4. Expression of Can1-Mars provokes a slow growth phenotype. (A) Growth assay comparing Mup1-GFP-FKBP and Can1-GFP-FKBP strains (without Mup1-Mars or Can1-Mars) with a WT strain. All exhibited normal growth. Image was taken after incubation at 26°C for 3 d. **(B)** Growth assay comparing Mup1-GFP-FKBP strains with a WT strain. Strain 2 exhibited normal growth. Strain 3 displayed a slow growth phenotype. Image was taken after incubation at 26°C for 2 d. **(C)** Growth assay comparing Can1-GFP-FKBP strains with a WT strain. Strain 2 exhibited normal growth. Strain 3 displayed a slow growth phenotype. Image was taken after incubation at 26°C for 3 d.

Table S1. Yeast strains used in this study.

Name	Genotype	Source
SEY6210	*MATα ura3-52 his3-200 leu2-3,112 trp1-901 lys2-801 suc2-9*	Robinson et al., 1988
RSY62	SEY6210, *VPH1-mCHERRY::HIS3*	Sardana et al., 2018
RSY67	SEY6210, *ssh4Δ::NATMX6*	Richa Sardana
RSY130	SEY6210, *VPH1-mCHERRY::HIS3 MUP1-pHluorin::LEU2 ssh4Δ::KANMX6 ear1Δ::NATMX6*	Sardana et al., 2018
RSY131	SEY6210, *VPH1-mCHERRY::HIS3 WSC1-GFP::LEU2*	Sardana et al., 2018
RSY132	SEY6210, *VPH1-mCHERRY::HIS3 WSC1-GFP::LEU2 ssh4Δ::NATMX6*	Sardana et al., 2018
RSY133	SEY6210, *VPH1-mCHERRY::HIS3 WSC1-GFP::LEU2 ssh4Δ::KANMX6 ear1Δ::NATMX6*	Sardana et al., 2018
RSY183	SEY6210, *end3Δ::HIS3*	Sardana et al., 2018
RSY190	SEY6210, *URA3 VPH1-mCHERRY::HIS3 WSC1-GFP::LEU2*	Richa Sardana
RSY247	SEY6210, *VPH1-mCHERRY::HIS3 ssh4Δ::NATMX6 WSC1-acLL-GFP::LEU2*	Sardana et al., 2018
RSY336	SEY6210, *MUP1-GFP-2xFKBP::TRP1 FRB-SSH4::URA3 tor1-1 fpr1Δ::NATMX6*	This study
RSY340	SEY6210, *MUP1-GFP::TRP1 FRB-SSH4::URA3 tor1-1 fpr1Δ::NATMX6*	This study
RSY415	SEY6210, *CAN1-GFP-2xFKBP::TRP1 tor1-1 fpr1Δ::NATMX6*	This study

Table S2. Plasmids used in this study.

Name	Sequence	Source
pRS85	*WSC1-GFP URA3 CEN*	Richa Sardana
pRS86	*WSC1-acLL-GFP URA3 CEN*	Sardana et al., 2018
pRS109	*PMA1-GFP URA3 CEN*	Richa Sardana
pRS120	*PMA1-GFP-acLL URA3 CEN*	Richa Sardana
pRS110	*MID2-GFP URA3 CEN*	Richa Sardana
pRS112	*MID2-GFP-acLL URA3 CEN*	Richa Sardana
pRS171	*VHT1-GFP URA3 CEN*	Richa Sardana
pRS202	*VHT1-acLL-GFP URA3 CEN*	Richa Sardana
pRS172	*SUR7-GFP URA3 CEN*	Richa Sardana
pRS185	*SUR7-GFP-acLL URA3 CEN*	This study
pRS203	*SUR7-acLL-GFP URA3 CEN*	Richa Sardana
pRS173	*GPA1-GFP URA3 CEN*	Richa Sardana
pRS186	*GPA1-GFP-acLL URA3 CEN*	This study
pRS204	*GPA1-acLL-GFP URA3 CEN*	Richa Sardana
pRS174	*MEP2-GFP URA3 CEN*	Richa Sardana
pRS187	*MEP2-GFP-acLL URA3 CEN*	This study
pRS205	*MEP2-acLL-GFP URA3 CEN*	Richa Sardana
pRS201	*YOR1-GFP URA3 CEN*	Richa Sardana
pRS208	*YOR1-acLL-GFP URA3 CEN*	Richa Sardana
pEG162	*MUP1-GFP LEU2 CEN*	Guiney et al., 2016
pRS82	*MUP1-acLL-GFP LEU2 CEN*	Sardana et al., 2018
pRS105	*MUP1(K16,27,28R)-acLL-GFP LEU2 CEN*	Richa Sardana
pRS275	*MUP1(K27,28R)-acLL-GFP LEU2 CEN*	Richa Sardana
pRS368	*SSH4 URA3 CEN*	This study
pRS369	*SSH4(PY) URA3 CEN*	This study
pRS370	*EAR1 URA3 CEN*	This study
pRS371	*EAR1(PY) URA3 CEN*	This study
pRS374	*EAR1 TRP1 CEN*	This study
pRS375	*EAR1(PY) TRP1 CEN*	This study
pRS401	*EAR1-SSH4SPRY URA3 CEN*	This study
pRS403	*SSH4-EAR1SPRY URA3 CEN*	This study
pRS390	*SSH4-EAR1SPRY-NEONGREEN-3xHA URA3 CEN*	This study
pRS175	*SSH4-NEONGREEN-3xHA URA3 CEN*	Richa Sardana
pRS191	*WSC1-acLL-MARS LEU2 CEN*	Richa Sardana
pRS428	*SSH4-GFP URA3 CEN*	Richa Sardana
pRS524	*SSH4-GFP-KKTN URA3 CEN*	This study
pRS525	*SSH4-RCR1(CTAIL)-GFP URA3 CEN*	This study
pRS530	*MUP1-MARS LEU2 CEN*	This study
pRS597	*FRB-SSH4 URA3 CEN*	This study
pRS622	*FRB-SSH4 LEU2 CEN*	This study
pRS638	*CAN1-MARS LEU2 CEN*	This study